# Hybrid Multibeamforming Receiver With High-Precision Beam Steering for Low Earth Orbit Satellite Communication

Ye-Eun Chi, Jinki Park, and Seong-Ook Park, *Senior Member, IEEE*

***Abstract*— A hybrid multibeamforming receiver for low Earth orbit (LEO) satellite communication in the Ku-band is designed and tested. The proposed receiver is implemented with eight channels to enable the multibeam control. The proposed receiver, including both analog and digital beamforming structures, is capable of multibeam reception using both analog and digital beamforming techniques simultaneously or selectively. Analog beamforming is implemented by employing a local oscillator phase shifter using direct digital synthesis and phase-locked loop (PLL) structures. In digital beamforming, a software-defined radio can control the phase of the signal in the digital baseband. The multibeam received using the proposed hybrid multibeamforming receiver was measured at 11.7 and 12.7 GHz in an anechoic chamber. The phase-control resolutions of analog and digital beamforming were 0.022° and 0.72°, respectively. Analog beam-switching speed is slower than digital beamforming because it depends on the settling time of the PLL circuit, but it has a high phase-control resolution. Therefore, by using analog and digital beamforming when precise beam tilting and fast beam switching are required, respectively, the proposed hybrid multibeamforming is shown to be suitable in accordance with the communication situation.**

***Index Terms*— Analog beamforming, digital beamforming, hybrid multibeamforming, low Earth orbit (LEO) communication, multibeam.**

## I. Introduction

SATELLITES orbiting the Earth are classified into geostationary orbit [or geosynchronous equatorial orbit (GEO)], medium Earth orbit (MEO), and low Earth orbit (LEO) depending on the altitude. In recent years, LEO satellite communication has witnessed new developments [1], [2], [3], [4], [5]. With increasing interest in LEO satellites, SpaceX, OneWeb, Telesat, and Amazon are actively building a global Internet network [6], [7], [8], [9], [10], [11]. LEO satellites are located at an altitude of ∼160–2000 km, enabling wireless communication even in remote areas without base stations. Compared to other satellite communications, in LEO, the free-space path loss between the satellite and the terminal is reduced because of the low altitude. This characteristic affords the advantages of a low transmission-delay rate and reduction in the size of the terminal antenna. However, unlike GEO satellites, in which satellites appear to be fixed over the Earth, LEO satellites periodically change their positions over the Earth. Consequently, reliable communication that continuously connects one satellite and a base station on the Earth is almost impossible in LEO. In addition, LEO satellites have lower antenna-beam coverage on the Earth, as the altitude is lower than those of GEO and MEO satellites [6], [7], [8]. Therefore, several LEO satellites are required to match the coverage of one GEO satellite.

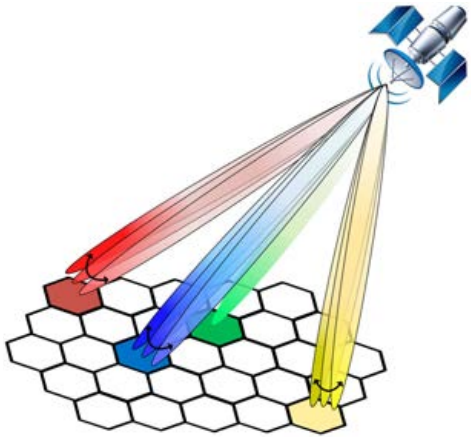

Fig. 1. Multibeamforming technology for LEO satellite communication.

The simplest method for increasing the coverage and stability of communication using LEO satellites is using a large number of satellites. As the number of satellites increases, the coverage area increases. However, with the increase in the number of satellites, problems of frequency interference, intersatellite collision, and complexity of intersatellite link communication may occur. Therefore, instead of increasing the number of satellites, the development of multibeam technology has become a trend. Fig. 1 shows a schematic of multibeamforming technology for LEO satellites. The multibeamforming is a technology that combines multibeam and beamforming technology. Multibeam technology is essential for improving communication quality in LEO satellites [12], [13], [14], [15], [16]. Multibeam technology refers to forming a plurality of independent beams instead of a single beam using one antenna [17], [18]. A multibeam-equipped LEO satellite facilitates

Manuscript received 10 September 2022; revised 10 April 2023; accepted 20 April 2023. Date of publication 22 May 2023; date of current version 7 July 2023. This work was supported by a grant-in-aid of HANWHA SYSTEMS. *(Corresponding author: Ye-Eun Chi.)*

The authors are with the Microwave and Antenna Laboratory, School of Electrical Engineering, Korea Advanced Institute of Science and Technology (KAIST), Daejeon 34141, South Korea (e-mail: yechi@kaist.ac.kr; psisquare@kaist.ac.kr; soparky@kaist.ac.kr).

Color versions of one or more figures in this article are available at https://doi.org/10.1109/TAP.2023.3277195.

Digital Object Identifier 10.1109/TAP.2023.3277195

improvement in communication coverage through a plurality of beams. The beamforming technique as well as the multibeam is an important part in satellite communication. The beamforming technique using an array antenna involves controlling the beam angle. Application of the beamforming technique to each multibeam enables beam tracking for a target. This helps to overcome the difficulties of continuous communication and implement stable communication. Therefore, multibeamforming improves coverage and transmission capacity and can help build a reliable communication network. Moreover, a multibeamforming system can be implemented using passive and active multibeamforming [18], [19], [20], [21], [22]. In passive multibeamforming, the number and direction of beams are predetermined. By contrast, active multibeamforming electronically controls the beam, forming and tilting it whenever necessary. LEO satellites require active multibeamforming for stable communication according to their movement [23], [24]. Active multibeamforming architecture is divided into analog and digital. An analog multibeamforming structure is typically designed using a phase shifter. The phase shifter is located at the radio frequency (RF), local oscillator (LO), and intermediate frequency (IF) stages to control the phase of the signal; therefore, it can be used in various system structures [25], [26], [27], [28], [29], [30]. In a receiver, it can be placed before or after a low-noise amplifier (LNA) to compensate for phase changes caused by the amplifier. In addition, because of the simplicity of the system structure, implementing it is relatively easy compared to other beamforming structures. However, current commercial technology limits the control resolution of phase-shifting devices to 2.8° [31], [32]. Such an analog multibeamforming technique is ineffective in terms of system performance and economic feasibility because of the limited resolution of the phase-shift device and expensive components. In a digital multibeamforming structure, signal processing is possible at the digital baseband signal part instead of the phase-shift device of the RF front end [13], [33], [34]. These advantages of signal processing enable techniques such as ultralow sidelobes, enhanced adaptive pattern nulling, and multiple simultaneous beams that are difficult to realize with other architectures [35], [36], [37]. However, if the multibeam is implemented only with a digital beamforming structure, several difficulties arise, e.g., design complexity and power consumption. Hybrid multibeamforming is an optimized system structure based on the advantages and disadvantages of analog and digital beamforming techniques, being a combination of the two [38]. The various hybrid beamforming techniques have been developed [38], [55], [56], [57]. Among hybrid beamforming techniques, the analog beamforming consists of power divider and phase shifters [55], [56]. This is possible to reduce the number of transceivers by finding an optimized beamforming network in analog and digital. However, the analog beamformer is bulky and expensive due to multiple phase shifters. In the case of hybrid radar, the transmitter and receiver can implement only analog and digital beamforming, respectively [38]. The orthogonal hybrid multibeam array antenna consists of a buttler matrix with a passive beamforming network and a digital beamformer [57]. Using this array antenna, passive multibeam with fixed beam spacing was implemented in the vertical direction and digital beamforming in the horizontal direction. That is, the analog and digital beamforming is determined according to the direction.

In this article, we propose a multibeamforming receiver with a hybrid structure that combines direct digital synthesis (DDS)-based analog and digital beamforming. The analog beamforming system overcomes low phase-control resolution and insertion loss by using the virtual phase shifter of the LO stage instead of the phase shifter of the RF stage. In the proposed digital beamformer, the amplitude and phase of signals are controlled using software-defined radio (SDR) such as the field-programmable gate array (FPGA), HackRF one for fast beam switching. In addition, the proposed receiver can select one of the analog and digital beamforming methods or simultaneously implement analog and digital beams by using both. Using the beamforming measurement setup in the anechoic chamber, we analyze and evaluate the performance of the proposed eight-channel hybrid multibeamforming receiver.

This article is organized as follows. The principle of the hybrid multibeamforming system is introduced in Section II. Section III describes the eight-channel hybrid multibeamforming receiver architecture. In Section IV, multibeamforming results obtained from an eight-channel hybrid receiver in an anechoic chamber are analyzed and discussed. Finally, conclusions are drawn in Section V.

## II. Principle of the Hybrid Multibeamforming System

Hybrid multibeamforming is a technique that combines analog and digital beamforming. This section describes each of the analog and digital beamforming techniques for achieving the principle of hybrid beamforming.

### *A. DDS–Phase-Locked Loop Structure for Phase Control Based on Analog Beamforming*

In the analog beamforming structure, the virtual phase-shifter-based LO signal is used for high-precision phase control. The virtual phase shifter is implemented by combining the DDS and phase-locked loop (PLL) techniques [39], [40], [41], [42]. The PLL technique is employed for the LO signal generation part to maintain the high phase-control resolution of the DDS, which has a frequency limit [43], [44]. In addition, a phase-controllable LO signal without degradation due to the phase noise is achieved using DDS-driven PLL synthesizers. Fig. 2 shows the architecture of the LO signal generator with high phase-control resolution using DDS and two phase detectors based on the PLL circuit. The two phase detectors are used for signal generation for phase comparison with DDS and for signal synchronization. The circuit for phase locking of the LO signal comprises a voltage-controlled oscillator (VCO), sampling phase detector (SPD), reference signal ($y_{REF}$) for SPD, phase frequency detector (PFD), charge pump (CP), loop filter (LF), and DDS for the reference signal of the PFD. As the first stage of the PLL, the reference signal ($y_{REF}$) input to the SPD passes through a frequency doubler, and a signal ($y_{2REF}$)

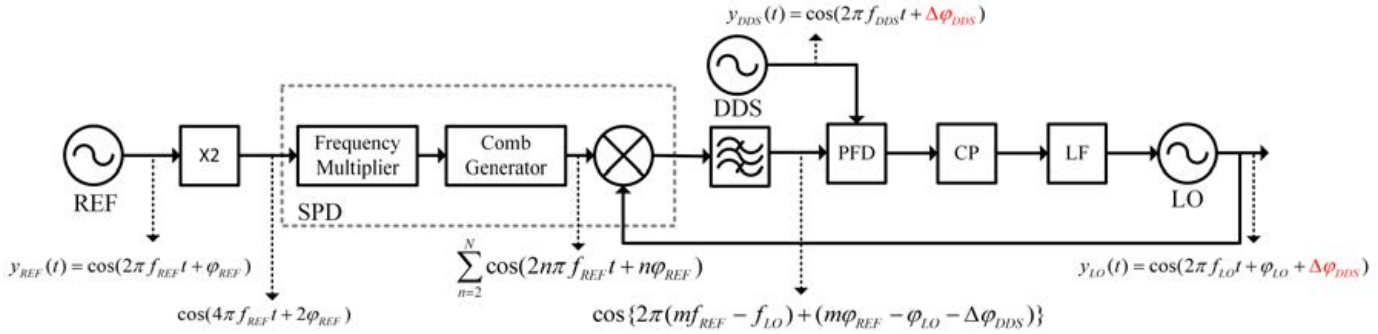


Fig. 2. LO signal generator with high phase-control resolution using two phase detectors.

with twice the frequency and phase is generated as follows:

$$y_{REF}(t) = A_{REF}\cos(2\pi f_{REF}t + \varphi_{REF}) \quad (1)$$

$$y_{2REF}(t) = A_{2REF}\cos(4\pi f_{REF}t + 2\varphi_{REF}) \quad (2)$$

where $A_{REF}$, $f_{REF}$, and $\varphi_{REF}$ are the amplitude, frequency, and phase, respectively, of the reference signal for SPD and $A_{2REF}$ is the amplitude of the signal passing through the frequency doubler. To generate the harmonic signals, the signal passing through the frequency doubler is passed though the frequency multiplier and comb generator inside the SPD. The harmonic signals can be represented as follows:

$$y_{SPD} = \sum_{n=2}^{N} A_n\cos(2n\pi f_{REF}t + n\varphi_{REF}) \quad (3)$$

where $n$ denotes the number of harmonic signals. The SPD output signal is generated by frequency mixing of the harmonic signals ($y_{SPD}$) and the VCO signal input to the SPD. To compare only the desired frequency in the PFD, the SPD output signals are passed through a bandpass filter (BPF). After the SPD part, the PFD compares the frequency and phase of the two input signals. In the PFD, the DDS signal is used as a reference signal and the SPD output signal is used as an RF signal for comparison. The SPD output signal is synchronized according to the frequency and phase of the DDS signal in the PFD. Therefore, the phase of the VCO changes as much as that of the DDS signal changes. The DDS and VCO signals are given as follows:

$$y_{DDS}(t) = A_{DDS}\cos(2\pi f_{DDS}t + \Delta\varphi_{DDS}) \quad (4)$$

$$y_{LO}(t) = A_{LO}\cos(2\pi f_{LO}t + \varphi_{LO} + \Delta\varphi_{DDS}) \quad (5)$$

where $A_{DDS}$, $f_{DDS}$, and $\Delta\varphi_{DDS}$ are the amplitude, frequency, and phase, respectively, of the DDS output signal and $A_{LO}$, $f_{LO}$, and $\varphi_{LO}$ are the amplitude, frequency, and phase, respectively, of the VCO signal for the LO signal.

### B. LO Phase Shifter Based on Analog Beamforming

A simple block diagram of the frequency direct-conversion receiver is shown in Fig. 3. Because of the DDS–PLL architecture, the phase of the LO signal depends on the phase of the DDS signal, which is the reference signal of the PFD.

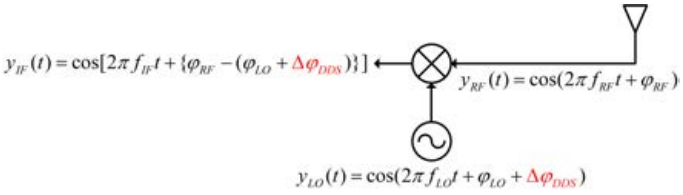


Fig. 3. Block diagram of the frequency direct-conversion receiver using an LO phase shifter.

The signal ($y_{RF}$) received from the antenna is expressed as follows:

$$y_{RF}(t) = A_{RF}\cos(2\pi f_{RF}t + \varphi_{RF}) \quad (6)$$

where $A_{RF}$, $f_{RF}$, and $\varphi_{RF}$ are the amplitude, frequency, and phase, respectively, of the RF signal received by the antenna. The RF signal is mixed with the LO signal in the frequency downconverting mixer. The output signal of the mixer can be expressed as follows:

$$y_{IF}(t) = A_{IF}\cos[2\pi f_{IF}t + \{\varphi_{RF} - (\varphi_{LO} + \Delta\varphi_{DDS})\}] \quad (7)$$

where $A_{IF}$, $f_{IF}$, and $\varphi_{IF}$ are the amplitude, frequency, and phase, respectively, of the IF signal as the output signal of the receiver. The frequency of the IF signal equals the difference in frequency between the LO and RF signals. The phase of the IF signal is changed linearly as much as the phase of the LO signal is controlled by the DDS. The proposed hybrid multibeamforming receiver maintains the high phase-control resolution of the DDS with a 14-bit phase offset resolution. In this work, the phase control resolution of the IF signal could be controlled with an interval of approximately 0.022° using DDS.

### C. Phase Control Based on Digital Beamforming

The digital beamforming receiver structure is shown in Fig. 4. It has the same RF front end as the proposed analog beamforming structure with the LO phase shifter. In the digital beamforming receiver—unlike analog beamforming—the IF signal passing through the frequency downconverting mixer is not summed in the RF combiner, and all signals are individually digitized by an analog-to-digital converter (ADC). A digital signal is converted into a quantized baseband signal

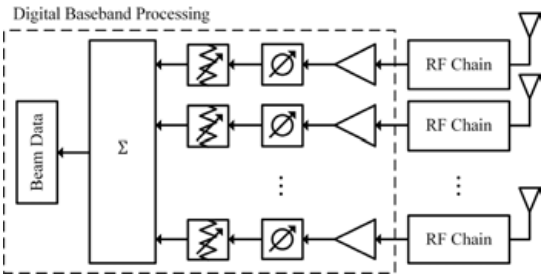


Fig. 4. Block diagram of the digital beamforming receiver.

through a digital downconverter (DDC). The amplitude and phase of the quantized signal can be changed through digital signal processing. Before implementing the beamforming technique, the amplitude and phase of the quantized signal should be calibrated for synchronization. The calibrated eight-channel baseband signals of digital beamforming are expressed as follows:

$$\begin{aligned} s_1(t) &= w_1 A_1 \cos(2\pi f t + \theta_1 + \varphi_1) \\ s_2(t) &= w_2 A_2 \cos(2\pi f t + \theta_2 + \varphi_2) \\ &\vdots \\ s_8(t) &= w_8 A_8 \cos(2\pi f t + \theta_8 + \varphi_8) \end{aligned} \tag{8}$$

where $A_1$, $f$, and $\theta_1$ are the amplitude, frequency, and phase, respectively, of the baseband signal of the first channel; $A_2$ and $\theta_2$ are the amplitude and phase, respectively, of the baseband signal of the second channel; and $A_8$ and $\theta_8$ are the amplitude and phase, respectively, of the baseband signal of the eighth channel. Further, $w_1$, $w_2$, and $w_8$ are weighting factors for the amplitude of the baseband signal of the first, second, and eighth channels, respectively, and $\varphi_1$, $\varphi_2$, and $\varphi_8$ are the weighting factors for the phase of the baseband signal of the first, second, and eighth channels, respectively. Signals of all channels independently have the weighting factor by digital signal processing. Therefore, digital beamforming is implemented by setting weighting factors for beam tilting as well as calibration. We used an SDR including an ADC and DDC for digital signal processing.

### D. Analysis of Beam-Switching Speed

Because beamforming is implemented through a phase change between array antennas, the beam-switching speed is the same as the time taken for the phase to change. The beam-switching speed of the proposed analog beamforming technique depends on the settling time of the PLL circuit, which is directly proportional to its PFD update period [45]. The PFD used in the PLL circuit comprises two D flip-flops and a programmable delay element. The RF and reference signals for comparing the frequency and phase are input to the two D flip-flops. The output signals of the two D flip-flops are fed to the CP. The programmable delay element of the PFD controls the width of the antibacklash pulse. This pulse minimizes phase noise and reference spurs. However, the beam-switching speed is also affected by this pulse. Fig. 5 shows the measured settling time for phase locking of the

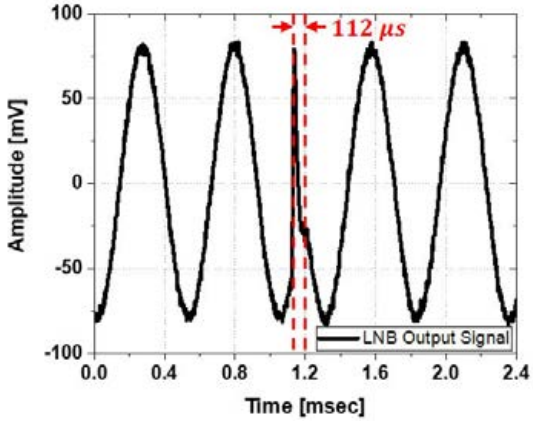


Fig. 5. Measured settling time for phase locking using LO phase shifter with the DDS–PLL technique.

low-noise block downconverter (LNB) having the structure shown in Figs. 2 and 3. To measure the settling time, the proposed LNB with the LO phase shifter using the DDS–PLL technique and a universal software radio peripheral (USRP) was used. The settling time was calculated as the time taken for the phase of the sine wave to change by analyzing the IF output signal of the LNB received from the USRP. As described earlier, the phase of the output signal of the LNB depends on the phase of the DDS. Therefore, the phase-fixed settling time was measured by controlling the phase of the DDS. When the phase of the signal output from the DDS was changed from 0° to 180°, the time taken for the phase to be fixed was 112 $\mu$s. Therefore, the beam-switching speed using the proposed analog beamforming technique was 112 $\mu$s.

In the proposed digital beamforming technique, the phase of the signal was controlled by digital processing. In the receiver using the digital beamforming structure, the IF signal, which is the output signal of LNB, was monitored and measured in the SDR. Fig. 6 shows the measured settling time for phase locking after digital signal processing. When the phase of the signal was shifted by 90° using digital signal processing, the time taken for the phase of the IF signal to change was 8.33 $\mu$s. Then, the beam-switching speed using the proposed digital beamforming technique was 8.33 $\mu$s. Regarding the beam-switching speed, the proposed digital beamforming technique was verified to be faster than the proposed analog beamforming technique.

## III. Design of the Hybrid Multibeamforming System

This section analyzes the structure of the hybrid multibeamforming receiver system. We designed and fabricated the eight-channel receiver for hybrid multibeamforming.

### A. System Architecture

The overall schematic of the proposed hybrid multibeamforming system is shown in Fig. 7. The hybrid multibeamforming system was designed using the principles of analog and digital beamforming as described in Section II.

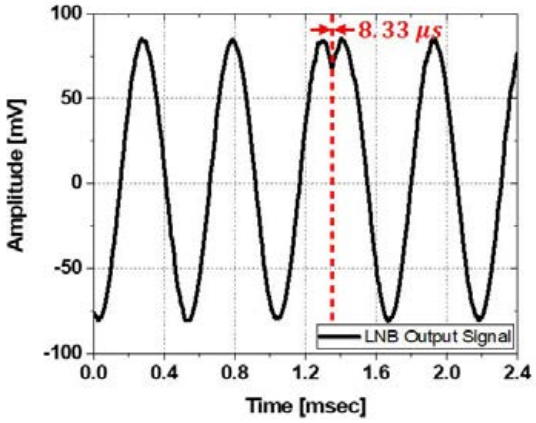


Fig. 6. Measured settling time for phase locking using SDR.

Independent beamforming was achieved through each beamforming method. The proposed hybrid multibeam-forming system comprises eight RF chains. The overall system has a 1 × 8 waveguide array antenna, RF front-end part, LO signal generator part, reference signal part, analog data acquisition and combiner part, and digital data acquisition and combiner part.

To implement multibeamforming, frequency and phase synchronization of the entire system is essential. The proposed system has a reference signal part for synchronization. Using a reference signal, the frequencies of all systems are synchronized. Beamforming is a technique that uses the interference effect of radio waves by varying the phase for each antenna. Therefore, before inputting the phase difference for each antenna, all signals received from the antenna must have the same phase. The calibration technique for signal phase synchronization was implemented using the DDS of the LO signal generator part in analog beamforming and digital data acquisition and combiner part in digital beamforming [35], [44], [58]. Fig. 8 shows eight channels synchronized using DDS. The IF signals of eight channels have almost the same amplitude and phase, as shown in Fig. 8. Similarly, in the case of digital beams, after eight-channel signals are synchronized, beamforming is implemented by controlling the phase difference.

### B. 1 × 8 Array Antenna Part

Fig. 9 shows the 1 × 8 waveguide array antenna prototype. The waveguide array antenna was used to validate the implementation of hybrid multibeamforming. The waveguide port of antenna has been widely used in satellite communication systems to reduce the loss of power. Therefore, the proposed receiver system with waveguide port can be combined with various antennas including the 1 × 8 waveguide array antenna. The size of a single waveguide antenna is 19.05 × 9.53 mm, which is the same as the waveguide standard WR75. To prevent structural interference between LNBs, the distance between antennas was kept at 43 mm. The size of the fabricated array antenna is 350 × 70 mm. The simulated and measured reflection coefficient of the waveguide array antenna is shown in Fig. 10 [46]. The measured reflection coefficient is −17.45 and −15.29 dB at 11.7 and 12.7 GHz, respectively. Further, the simulated and measured normalized radiation patterns of the array antenna are shown in Fig. 11. The measured antenna gain is 14.24 and 14.21 dBi at 11.7 and 12.7 GHz, respectively. The measured half-power bandwidth (HPBW) of the array antenna is 3.75° and 3.28° at 11.7 and 12.7 GHz, respectively. The specification of the array antenna is displayed in Table I.

TABLE I
ARRAY ANTENNA SPECIFICATION

| Parameter | 11.7 GHz | 12.7 GHz |
|---|---|---|
| Antenna gain | 14.24 dBi | 14.21 dBi |
| Reflection coefficient | −17.45 dB | −15.29 dB |
| Half-power bandwidth | 3.75 ° | 3.28 ° |
| Waveguide size | 19.05 mm × 9.53 mm | |
| Antenna size | 350 mm × 70 mm | |
| Gap between antennas | 43 mm | |

### C. RF Front-End Part

The RF front-end part after the antenna part comprises three LNAs, an RF BPF, and a mixer. From the antenna to the RF front-end part, the RF signal passes through the waveguide, so the insertion loss of the transmitted signal is low compared to that of the SMA cable. The substrate of RF front end is Rogers RO3003 with a permittivity of 3.0. The first part of the RF front-end part is the LNA, which comprises three stages to lower the noise figure of the entire system. The block diagram of the RF part of the LNB is shown in Fig. 12. The noise figure of the LNB is

$$F_{total} = F_1 + \frac{F_2 - 1}{G_1} + \frac{F_3 - 1}{G_1 G_2} + \frac{F_4 - 1}{G_1 G_2 G_3} + \frac{F_5 - 1}{G_1 G_2 G_3 G_4} \tag{9}$$

$$NF_{total} = 10 \log(F_{total}) \tag{10}$$

where $F_{total}$ and $NF_{total}$ are the cascaded noise factor and noise figure, respectively [50], [51]. $F_1$, $F_2$, $F_3$, $F_4$, and $F_5$ are the noise factors in the linear term of the first, second, and third LNA, BPF, and mixer, respectively. Further, $G_1$, $G_2$, $G_3$, $G_4$, and $G_5$ are the gains in the linear term of the first, second, and third LNA, BPF, and mixer, respectively. The cascaded noise figure and gain of the RF part of the LNB are 0.5 and 25.0 dB, respectively. One of the most important factors for receiver is the gain-to-noise temperature ratio (G/T). G/T is a value obtained by the gain of antenna with the noise temperature of the system [52], [53], [54]. When using the proposed basic waveguide array antenna, G/T is −1.49 dB. If an antenna with high gain is used, G/T can be expected to be improved.

Fig. 13 shows the geometry and simulated S-parameters of the designed BPF. BPF is designed as a microstrip line filter to pass only the desired frequency band [50]. The pass frequency band of BPF is 11.4–12.75 GHz, as shown in Fig. 13. The insertion loss is 1.5 dB at 12.0 GHz. The harmonic signals generated due to passage through the LNA are removed by the BPF of the LNB. The IF signal is generated by frequency down-conversion of the RF signal in the mixer. For signal

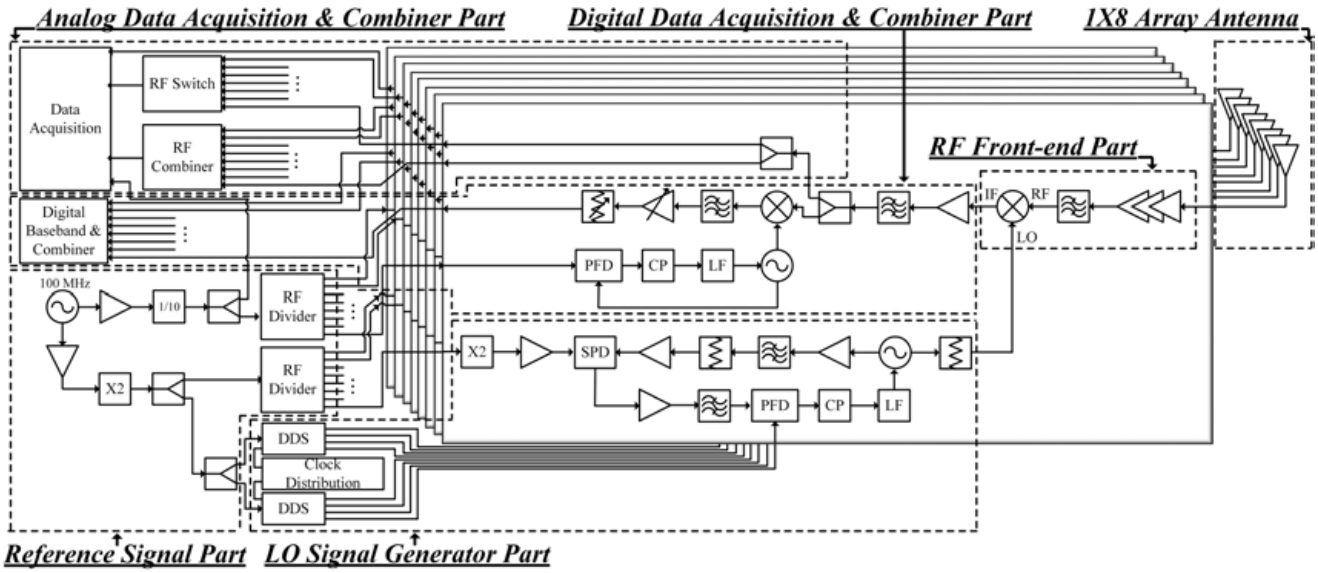


Fig. 7. Full architecture of the hybrid multibeamforming receiver.

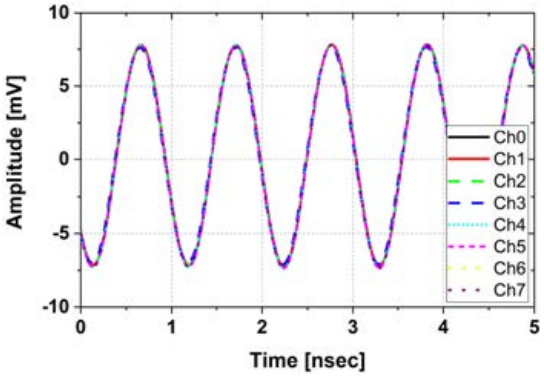


Fig. 8. Synchronization for eight-channel IF signals.

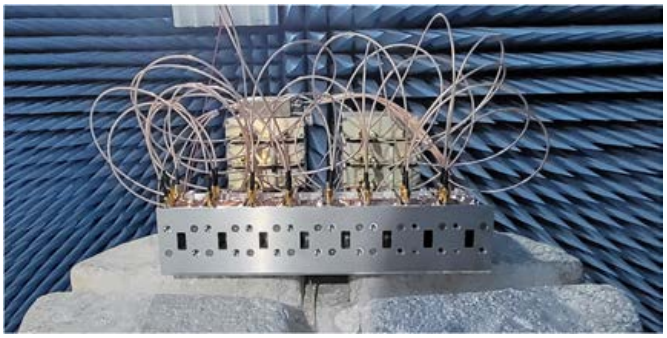

Fig. 9. Photograph of the 1 × 8 waveguide array antenna prototype.

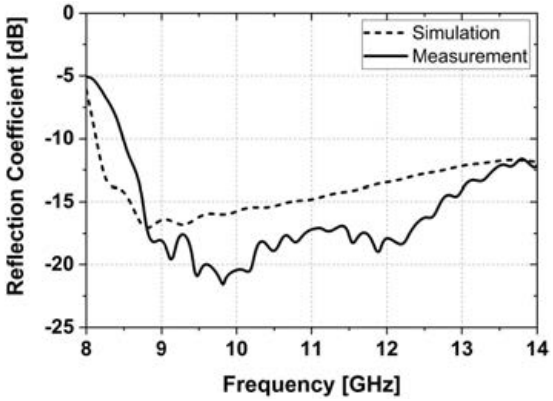


Fig. 10. Simulated and measured reflection coefficient of 1 × 8 waveguide array antenna.

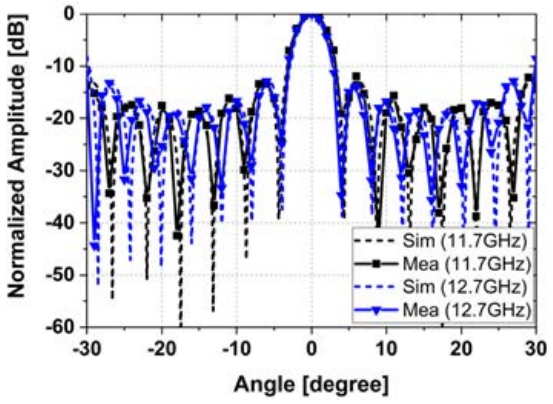


Fig. 11. Simulated and measured normalized radiation patterns of 1 × 8 waveguide array antenna.

synthesis for frequency down-conversion in the RF front end, a diode mixer was used [47], [48], [49]. Diode mixer is economical and has a simple structure. The characteristics of the frequency downconverted IF signal of the LNB with the designed BPF and mixer can be seen in Fig. 14. Fig. 14 shows the measured normalized power of the output signal of the RF front end.

### D. LO Signal Generator Part

The LO signal generator part of the proposed system is important in the analog beamforming technique. This part not only generates the LO signal used in the mixer, but also

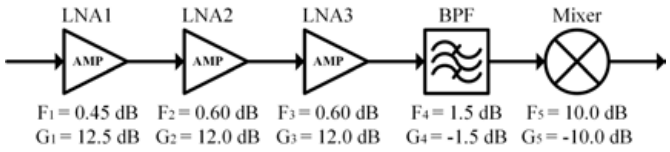


Fig. 12. Block diagram of the RF front-end part of LNB.

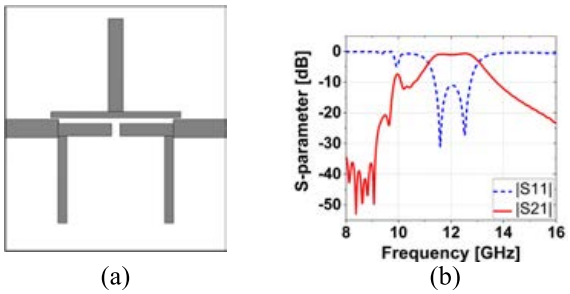


Fig. 13. Geometry and simulated S-parameters of the designed BPF: (a) geometry and (b) simulated S-parameters.

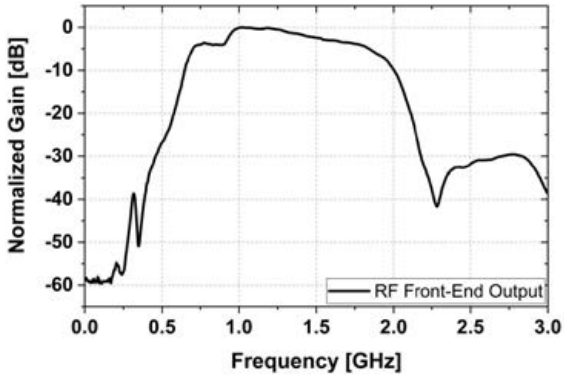


Fig. 14. Measured normalized power of output signal of RF front end.

controls the phase of the LO signal to implement the analog beamforming. The LO signal is generated using a 10.75-GHz VCO. SPD is used instead of the frequency divider used in the conventional PLL method. When the RF signal passes through a frequency divider, the frequency as well as the phase is multiplied. This has the effect of increasing the phase-control resolution. Therefore, SPD was introduced to maintain the high phase-control resolution. The 200-MHz signal generated from the reference signal part passes through the frequency doubler. The generated 400-MHz signal is input to the SPD. Using the frequency multiplier and comb generator inside the SPD, harmonic signals of 400 MHz are mixed with the LO signal in the mixer in the SPD. The frequency of the mixed signal is

$$f_{out}(t) = \sum_{n=1}^{\infty} (n\, f_{SPD\_ref}) - f_{LO} \tag{11}$$

where $f_{out}$, $f_{LO}$, and $f_{SPD\_ref}$ are the frequencies of the SPD output signal, LO signal, and reference signal input to the SPD, respectively, and $n$ is the number of harmonic signals. In this system, $f_{LO}$ and $f_{SPD\_ref}$ are 10.75 GHz and 400 MHz, respectively; therefore, the lowest frequency of the SPD output signal is 50 MHz when $n = 27$. The output signals of the SPD pass through the BPF centered at 50 MHz and are transmitted to the PFD. The frequency and phase of the LO signal are fixed using a PLL circuit comprising PFD, CP, and LF. The SPD output signal is input to the PFD, with the DDS signal used as a reference signal to fix the frequency and phase. To fix and control the frequency and phase for each LNB board of eight chains, eight channels of DDS signals are required. The AD9959, which has four output channels on one board provided by Analog Device Inc., was selected as the reference signal generator of PFD. It comprises four synchronized DDS cores with a sampling rate up to 500 million samples per second, and each channel provides independent frequency, phase, and amplitude control. Accordingly, we used two AD9959 boards for eight channels. Further, the frequency and phase of signal outputs from the two independent boards were synchronized using a separate clock distribution IC, namely, AD9510. The DDS generates a 50-MHz signal equal to the output signal of the SPD for frequency and phase locking in the PFD. Because the phase-control resolution of the DDS is 14 bit, the phase difference between channels can be controlled in intervals of approximately 0.022°. Therefore, as the SPD output signal is synchronized to the phase of the DDS signal in the PFD, the phase of the LO signal is changed by controlling the phase of the DDS.

### *E. Reference Signal Part*

To implement a multiple-input multiple-output technique such as beamforming, frequency synchronization between systems is important. If the frequencies are not synchronized, an error in the output signal may occur during signal synthesis. In the proposed system, a reference source signal of 100 MHz was used for frequency synchronization. The reference signal was used as the reference clock signal of the LO signal generator part, digital data acquisition and combiner part, and analog data acquisition and combiner part. In the LO signal generator part, the reference clock signal for the DDS and SPD input signal was of 200 MHz, generated by passing the reference source signal through a frequency doubler. The synchronization of the digital data acquisition and combiner part with the analog data acquisition and combiner part was implemented at 10 MHz, where the reference source signal was generated by passing through a 1/10 frequency divider. All reference signals passed through the power divider and were input to the LO signal generator part, digital data acquisition and combiner part, and analog data acquisition and combiner part to realize frequency synchronization.

### *F. Analog/Digital Data Acquisition and Combiner Part*

In the proposed receiver, the IF signal generated by the RF front-end part passes through a power divider to form a hybrid multibeam. The hybrid multibeam refers to the beams received using the analog and digital beamforming structures. The IF signals whose phase is controlled by the LO signal generator part are received by the analog data acquisition and combiner part. The analog data acquisition and combiner part includes RF switch, RF combiner, and data acquisition module. The

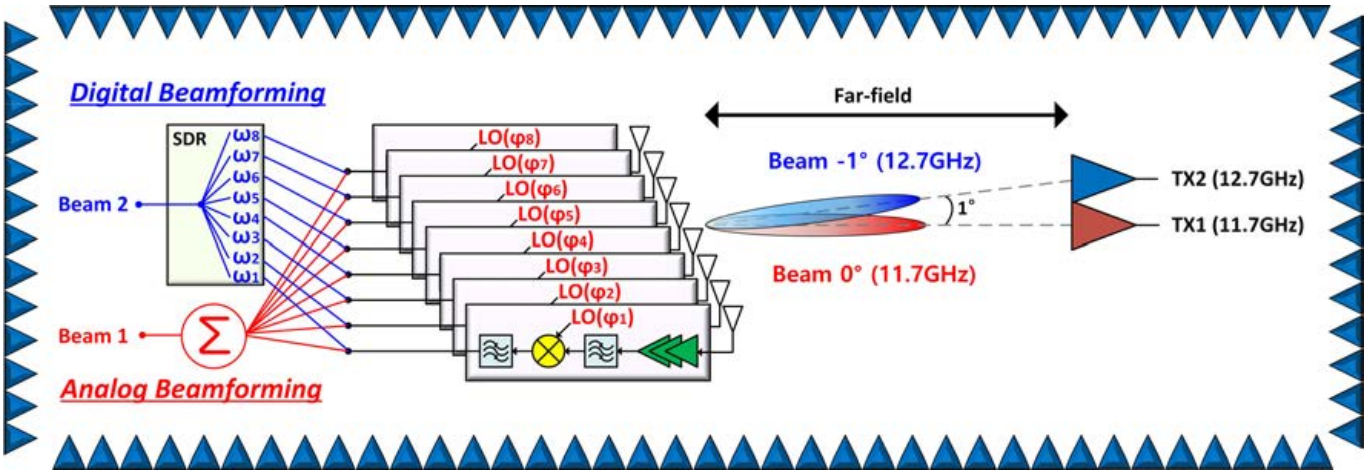


Fig. 15. Experimental method for simultaneously evaluating two multibeams.

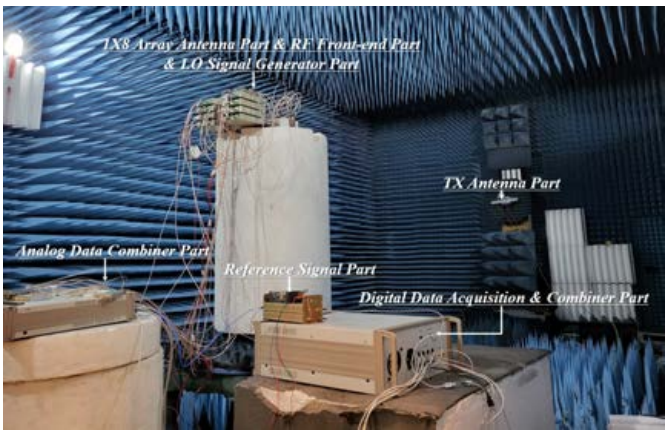


Fig. 16. Experimental setup for simultaneously measuring two multibeams.

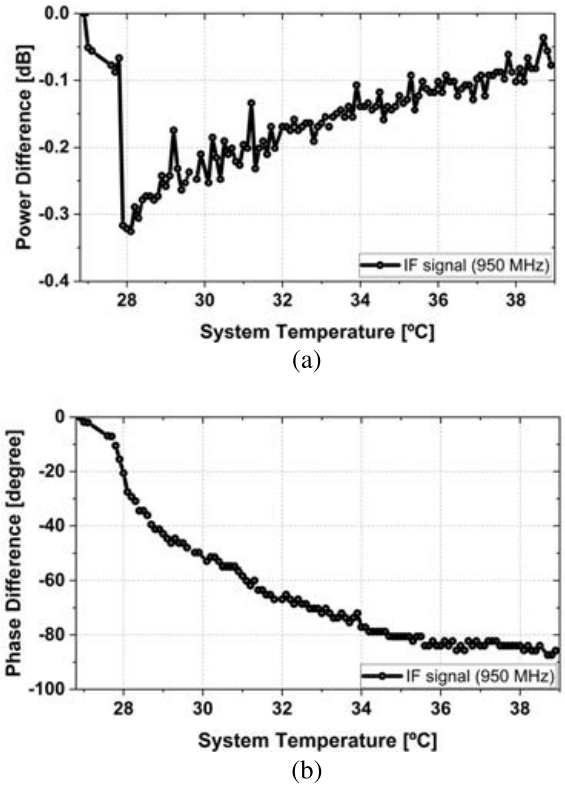


Fig. 17. Performance change of the proposed receiver system with temperature: (a) power difference and (b) phase difference.

RF switch is used for phase synchronization between IF signals and signal monitoring. The IF signal outputs from the eight-chain LNBs are synthesized and stored in the RF combiner and data acquisition module.

The digital data acquisition and combiner part includes digital combiner and eight pairs of mixers, variable amplifiers, and variable attenuators. In digital beamforming, the phase of the IF signal is controlled in the digital baseband. To control the signal in the digital baseband, the IF signal requires additional frequency down-conversion before the ADC and DDC. The frequencies and phases of the eight LO signals for additional down-conversion mixers in the digital data acquisition and combiner part are synchronized by the 10-MHz signal generated in the reference signal part. In the digital beamforming of the proposed receiver, the amplitude of the signals can be individually controlled in analog and digital basebands. The amplitude of the analog baseband signal passed through the additional mixer can be changed through the variable amplifier and variable attenuator. The amplitude of the digital baseband signal passed through the ADC and DDC is processed through digital signal processing. The phase of the signal can be controlled at 0.72° intervals in the digital baseband using SDR. Therefore, digital beams are formed in the following order. First, the IF signal of the LNB passes through the additional mixer, and the amplitude of the signal is primarily controlled through the amplifier and attenuator. The analog-based amplitude-controlled signal is digitized after passing through ADC and DDC. Thus, the amplitude and phase of the digital baseband signal can be controlled at the digital stage. Finally, digital beams are formed by combining the phase-controlled eight-channel digital baseband signals.

## IV. Measurement Results and Discussion

In this section, the multibeamforming experimental setup and results are presented. The proposed multibeamforming

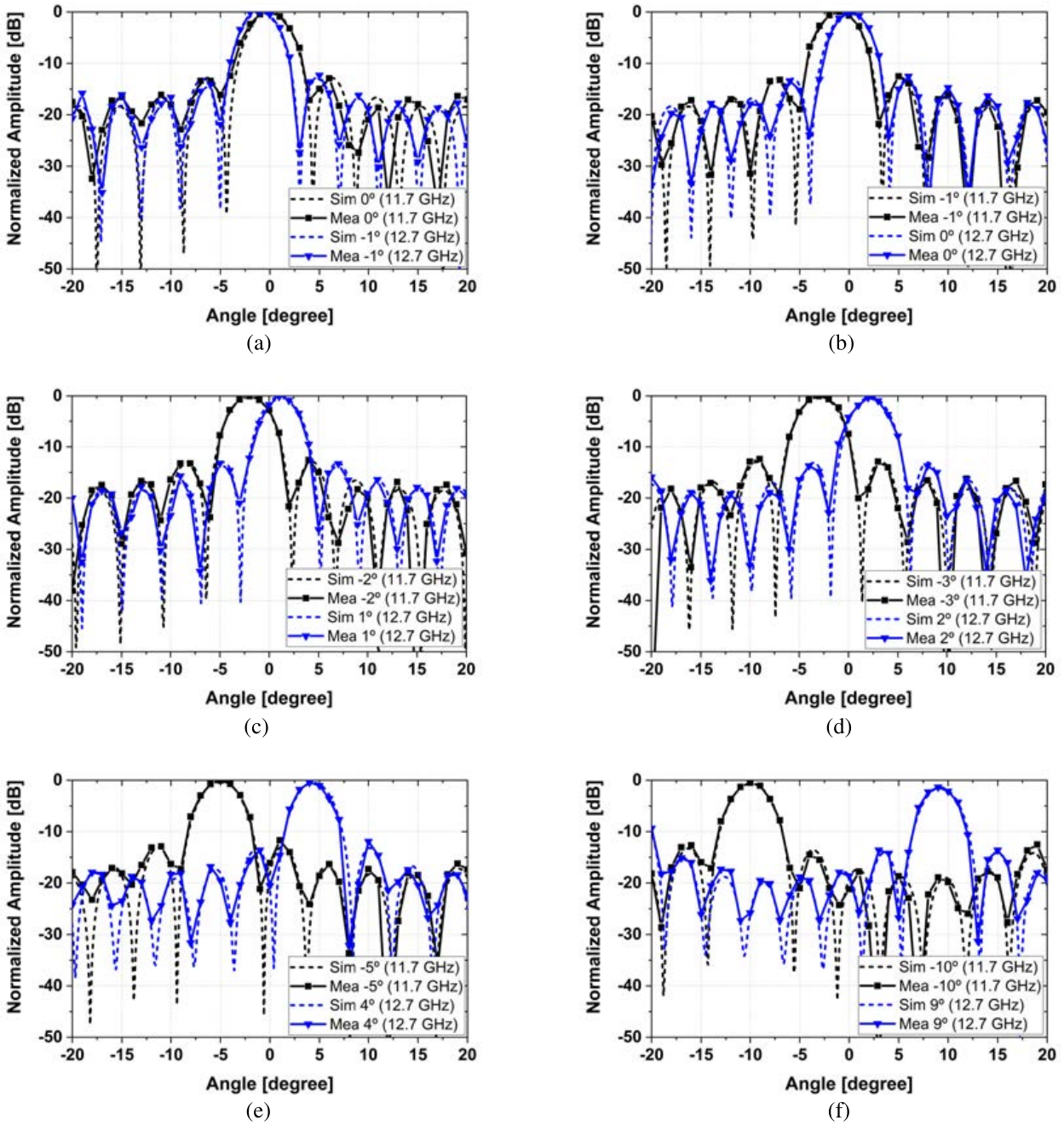


Fig. 18. Simulated and measured normalized radiation patterns for multibeamforming: (a) beam 0° (at 11.7 GHz) and beam −1° (at 12.7 GHz); (b) beam −1° (at 11.7 GHz) and beam 0° (at 12.7 GHz); (c) beam −2° (at 11.7 GHz) and beam 1° (at 12.7 GHz); (d) beam −3° (at 11.7 GHz) and beam 2° (at 12.7 GHz); (e) beam −5° (at 11.7 GHz) and beam 4° (at 12.7 GHz); and (f) beam −10° (at 11.7 GHz) and beam 9° (at 12.7 GHz).

receiver measured two multibeams simultaneously using the analog and digital beamforming structure.

### A. Experimental Setup

As described in Section III, a prototype of the eight-channel hybrid multibeamforming system was fabricated and evaluated. The proposed system can simultaneously measure beams of two or more different frequencies. In an experiment, two beams of 11.7 and 12.7 GHz were measured using the analog and digital beamforming systems, respectively. Therefore, two transmit antennas were required to propagate two signals of different frequencies. Two WR75 waveguide antennas were used as transmit antennas.

Fig. 15 depicts the schematic layout of the experimental setup for simultaneously evaluating the multibeamforming. The distance between the two transmit antennas is 86 mm, so that the angle between the transmit antennas becomes 1° when looking at the transmit antennas in the hybrid multibeamforming receiver. Thus, the main beam of 11.7 and 12.7 GHz signals occurs at 0° and −1° with the proposed measurement method. Fig. 16 shows the experimental setup for measuring two multibeams simultaneously. To eliminate

the effect of the reflected signal, the multibeamforming experiment was conducted in an anechoic chamber.

### *B. Performance Change of the Receiver With Temperature*

The proposed receiver system includes an active device such as an LNA. Because the active device can control the current, the performance can change depending on the temperature of the device. This means that the system has nonlinearity. To apply a system with these characteristics to a phased array, the system calibration technique is required. Fig. 17 shows the amplitude and phase change of the output signal of the proposed receiver system according to the temperature. The power of the IF signal of 950 MHz, which was the output signal of the system, decreased sharply when the system was turned on; however, the power difference decreased as the temperature increased. After the system was turned on, the temperature of the system was maintained at a maximum temperature of 38.9 °C. The maximum power difference was approximately 0.33 dB. At the maximum temperature, the power difference of the system was approximately −0.08 dB. Further, the phase difference of the IF signal was obtained by comparing the two IF signals. One of the IF signals was set as a reference, and the phase change of the other IF signal was measured. The phase difference occurred abruptly as the temperature increased after the system operation. After the temperature reached 35 °C, the phase difference value became moderate and was maintained at approximately −85.0°. The maximum phase difference value was −85.8°.

In the proposed system, the power value changed negligibly with temperature, but the phase changed significantly. Unexpected phase changes are fatal to beamforming. Therefore, after the temperature of the system was saturated before the multibeamforming experiment, the eight-channel systems were calibrated. Receiver calibration is a technique that synchronizes the phases of the IF signal output from each LNB when the eight-channel systems receive the same RF signal. In the proposed analog beamforming structure, the phase differences between the first IF signal and the other IF signals were measured using the RF switch. The phases of all channels were synchronized using DDS according to the detected phase differences. In the proposed digital beamforming structure, digital signal processing was used for calibrating all channels.

### *C. Measurement Results of Hybrid Multibeamforming*

Two signals of different frequencies were simultaneously received in real time using the proposed hybrid beamforming structure. Multibeamforming was analyzed after the output signal of the eight-channel receiver was synchronized. Fig. 18 shows the simulated and measured radiation patterns for multibeamforming using the proposed system. When all receivers were phase-synchronized, as shown in Fig. 18(a), the main beams of 11.7 and 12.7 GHz were measured at 0° and −1°, respectively. At 11.7 GHz, analog beamforming was implemented and measured in a negative-angle direction, while at 12.7 GHz, digital beamforming was performed in a positive-angle direction. For ∓1° beamforming, the phase difference between the arrays was −10.65° and 11.44° at 11.7 and 12.7 GHz, respectively. Because the phase-control resolution of the proposed hybrid beamforming system was 0.022° and 0.72° at 11.7 and 12.7 GHz, respectively, phase control was sufficiently possible. The beamforming angles for 11.7 and 12.7 GHz were measured to be ∓1°, ∓2°, ∓3°, ∓5°, and ∓10°. The respective beamforming results are shown in Fig. 18(b)–(f). The phase difference between the arrays for implementing beamforming at 11.7 and 12.7 GHz is shown in Tables II–IV, respectively. Unlike the radiation patterns calculated at 0.001° intervals in the simulation, the radiation patterns in the experiment were measured at 1° intervals. Fig. 19 shows the measured antenna gain and efficiencies for beam steering at a different frequency. The gain and efficiency of the antenna decreased as the beam tilting angle increased, compared to the gain of beam 0°. Fig. 20 shows the measured normalized receiver system gains for beam steering at a different frequency. The gain in the pass frequency band of the proposed receiver is generally flat.

In the case of the proposed analog beamforming system, the RF signal has a high phase-control resolution of 0.022°

TABLE II
RF FRONT-END SPECIFICATION

| | LNA1 | LNA2 | LNA3 | BPF | Mixer |
|---|---|---|---|---|---|
| Model | NE325S01 | NE425S01 | NE425S01 | Microstrip line | CJ3401-HF |
| Noise figure [dB] | 0.45 | 0.60 | 0.60 | 1.5 | 10.0 |
| Gain [dB] | 12.5 | 12.0 | 12.0 | -1.5 | -10.0 |

TABLE III
PHASE DIFFERENCE BETWEEN THE ARRAYS AT 11.7 GHZ

| Beam angle | 0° | -1° | -2° | -3° | -5° | -10° |
|---|---|---|---|---|---|---|
| Phase difference | 0° | -10.65° | -21.06° | -31.70° | -52.72° | -104.8° |

TABLE IV
PHASE DIFFERENCE BETWEEN THE ARRAYS AT 12.7 GHZ

| Beam angle | 0° | 1° | 2° | 3° | 5° | 10° |
|---|---|---|---|---|---|---|
| Phase difference | 0° | 11.44° | 22.87° | 34.30° | 57.11° | 113.8° |

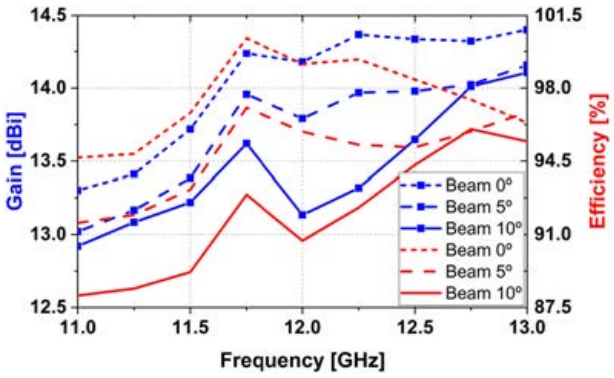


Fig. 19. Measured antenna gains and efficiencies for beam steering at a difference frequency.

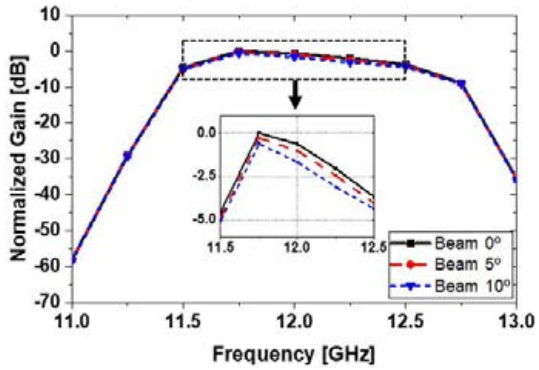


Fig. 20. Measured normalized receiver system gains for beam steering at a difference frequency.

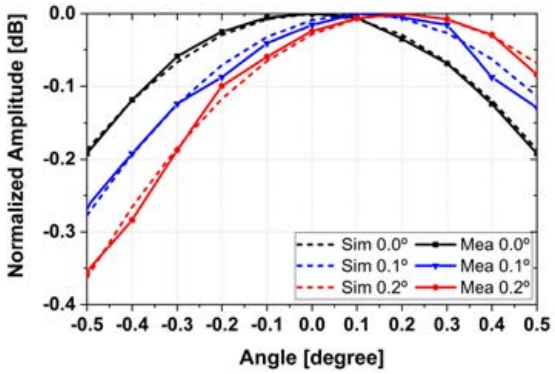


(a)

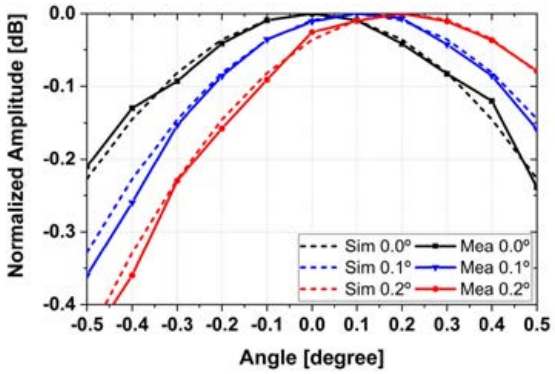


(b)

Fig. 21. Simulated and measured normalized radiation patterns with sophisticated beamforming: (a) 11.7 and (b) 12.7 GHz.

using the DDS–PLL structure. By using this system, performing precise beamforming at intervals of 0.1° is possible. Fig. 21 shows the simulated and measured radiation patterns for precise beamforming. In the measurement environment considering the array antenna spacing, the phase differences between the array antennas at 11.7 GHz for beamforming at 0.1° and 0.2° are 1.16° and 2.08°, respectively. Further, the phase differences between the array antennas at 12.7 GHz for beamforming at 0.1° and 0.2° are 1.26° and 2.29°, respectively. In the proposed system, beamforming at intervals of 0.1° was measured and confirmed in real time.

## V. Conclusion

A hybrid receiver with both analog and digital beamforming for multibeamforming has been proposed and discussed herein. The hybrid receiver includes LO phase-shifting technology using DDS for analog beamforming and SDR equal to the number of RF chains for digital beamforming. The analog beamforming technique was implemented by controlling the phase of the LO signal. The PLL circuit in the LO signal generator part was used to calibrate the frequency and phase between the eight chains of LNBs. By using the DDS with a high phase-control resolution as the reference signal of the PLL circuit, it was shown that the LO signal also maintained the high phase-control resolution. Therefore, precise beam tilting was confirmed to be possible using the analog beamforming technique. In the trend of an increase in wireless devices such as wearable devices, the proposed analog beamforming technique can precisely classify adjacent terminal antennas or mobile devices. When this technique is used with an antenna having a narrow beamwidth, precise beam tilting characteristics can be used more usefully. Among the proposed hybrid multibeamforming, the analog beamforming capable of high-precision beam steering can provide uninterrupted communication services to users. Further, the time taken for the phase of the LO signal to be controlled in the proposed receiver was measured. In the time taken for the phase of the LO signal to change, the PLL settling time dominates, so the beam-switching speed is rather slow. Digital beamforming has a lower phase-control resolution than the proposed analog beamforming technique. However, faster beam switching than that in the proposed analog beamforming technique is possible by digital signal processing. Fast beam switching can be applied to detection and tracking techniques. For example, among the proposed hybrid multibeamfomring, the digital beamforming technique can quickly find users using fast beam switching. It also reduces the communication delay that occurs during the time the beam is switched, thus enabling a reliable communication network. The proposed digital beamforming is suitable for satellite communication requiring multibeam technique because it can simultaneously receive and beam tilt multiple beams without additional systems.

To clarify that the proposed receiver implements analog and digital beamforming simultaneously, multibeamforming was analyzed at 11.7 and 12.7 GHz. Two multibeams having different frequencies were independently beam-tilted at 0° to $\mp 10°$. In addition, in analog beamforming with high phase-control resolution, the beam was confirmed to tilt at 0.1° intervals. Therefore, the proposed hybrid receiver can be used flexibly according to the required communication characteristics, such as fast beam switching or fine beam tilting. We expect the hybrid multibeamforming technique to be practically utilized in LEO satellite communication and 5G/6G mobile communication.

## References

[1] R. Kumar and S. Arnon, "SNR optimization for LEO satellite at sub-THz frequencies," *IEEE Trans. Antennas Propag.*, vol. 70, no. 6, pp. 4449–4458, Jun. 2022.

[2] F. S. Prol et al., "Position, navigation, and timing (PNT) through low earth orbit (LEO) satellites: A survey on current status, challenges, and opportunities," *IEEE Access*, vol. 10, pp. 83971–84002, 2022.

[3] T. Darwish, G. K. Kurt, H. Yanikomeroglu, M. Bellemare, and G. Lamontagne, "LEO satellites in 5G and beyond networks: A review from a standardization perspective," 2021, *arXiv:2110.08654*.

[4] A. Lalbakhsh, A. Pitcairn, K. Mandal, M. Alibakhshikenari, K. P. Esselle, and S. Reisenfeld, "Darkening low-earth orbit satellite constellations: A review," *IEEE Access*, vol. 10, pp. 24383–24394, 2022.

[5] J. M. Gongora-Torres, C. Vargas-Rosales, A. Aragón-Zavala, and R. Villalpando-Hernandez, "Link budget analysis for LEO satellites based on the statistics of the elevation angle," *IEEE Access*, vol. 10, pp. 14518–14528, 2022.

[6] T. G. Reid, A. M. Neish, T. F. Walter, and P. K. Enge, "Leveraging commercial broadband LEO constellations for navigating," in *Proc. ION GNSS*, Portland, OR, USA, Sep. 2016, pp. 2300–2314.

[7] S. Cioni, R. De Gaudenzi, O. D. R. Herrero, and N. Girault, "On the satellite role in the era of 5G massive machine type communications," *IEEE Netw.*, vol. 32, no. 5, pp. 54–61, Sep. 2018.

[8] I. Leyva-Mayorga et al., "LEO small-satellite constellations for 5G and beyond-5G communications," *IEEE Access*, vol. 8, pp. 184955–184964, 2020.

[9] M. Neinavaie, J. Khalife, and Z. M. Kassas, "Acquisition, Doppler tracking, and positioning with starlink LEO satellites: First results," *IEEE Trans. Aerosp. Electron. Syst.*, vol. 58, no. 3, pp. 2606–2610, Jun. 2022.

[10] J. Khalife, M. Neinavaie, and Z. M. Kassas, "The first carrier phase tracking and positioning results with starlink LEO satellite signals," *IEEE Trans. Aerosp. Electron. Syst.*, vol. 58, no. 2, pp. 1487–1491, Apr. 2022.

[11] L. You et al., "Hybrid analog/digital precoding for downlink massive MIMO LEO satellite communications," *IEEE Trans. Wireless Commun.*, vol. 21, no. 8, pp. 5962–5976, Aug. 2022.

[12] N. Anselmi, P. Rocca, M. Salucci, and A. Massa, "Contiguous phase-clustering in multibeam-on-receive scanning arrays," *IEEE Trans. Antennas Propag.*, vol. 66, no. 11, pp. 5879–5891, Nov. 2018.

[13] V. Ariyarathna et al., "Multibeam digital array receiver using a 16-point multiplierless DFT approximation," *IEEE Trans. Antennas Propag.*, vol. 67, no. 2, pp. 925–933, Feb. 2019.

[14] Y. Yeh and B. A. Floyd, "Multibeam phased-arrays using dual-vector distributed beamforming: Architecture overview and 28 GHz transceiver prototypes," *IEEE Trans. Circuits Syst. I, Reg. Papers*, vol. 67, no. 12, pp. 5496–5509, Dec. 2020.

[15] Q. Yu, W. Meng, M. Yang, L. Zheng, and Z. Zhang, "Virtual multi-beamforming for distributed satellite clusters in space information networks," *IEEE Wireless Commun.*, vol. 23, no. 1, pp. 95–101, Feb. 2016.

[16] J. Jing and C. Yu, "Multibeam digital predistortion for millimeter-wave analog beamforming transmitters," *IEEE Microw. Wireless Compon. Lett.*, vol. 30, no. 2, pp. 209–212, Feb. 2020.

[17] Y. Li, J. Wang, and K. Luk, "Millimeter-wave multibeam aperture-coupled magnetoelectric dipole array with planar substrate integrated beamforming network for 5G applications," *IEEE Trans. Antennas Propag.*, vol. 65, no. 12, pp. 6422–6431, Dec. 2017.

[18] W. Hong et al., "Multibeam antenna technologies for 5G wireless communications," *IEEE Trans. Antennas Propag.*, vol. 65, no. 12, pp. 6231–6249, Dec. 2017.

[19] K. Mori, "Multibeam antenna," U.S. Patent 7 388 552 B2, Jun. 17, 2008.

[20] Y. Yu, W. Hong, Z. H. Jiang, H. Zhang, and C. Guo, "Multibeam generation and measurement of a DDS-based digital beamforming array transmitter at Ka-band," *IEEE Trans. Antennas Propag.*, vol. 67, no. 5, pp. 3030–3039, May 2019.

[21] Y. Li and K. Luk, "A multibeam end-fire magnetoelectric dipole antenna array for millimeter-wave applications," *IEEE Trans. Antennas Propag.*, vol. 64, no. 7, pp. 2894–2904, Jul. 2016.

[22] A. Jouadé, S. Méric, O. Lafond, M. Himdi, and L. Ferro-Famil, "A passive compressive device associated with a Luneburg lens for multibeam radar at millimeter wave," *IEEE Antennas Wireless Propag. Lett.*, vol. 17, no. 6, pp. 938–941, Jun. 2018.

[23] G. He, X. Gao, L. Sun, and R. Zhang, "A review of multibeam phased array antennas as LEO satellite constellation ground station," *IEEE Access*, vol. 9, pp. 147142–147154, 2021.

[24] D. Sikri and R. M. Jayasuriya, "Multi-beam phased array with full digital beamforming for SATCOM and 5G," *Microw. J.*, vol. 62, no. 4, pp. 64–79, Apr. 2019.

[25] S. Moon, S. Yun, I. Yom, and H. L. Lee, "Phased array shaped-beam satellite antenna with boosted-beam control," *IEEE Trans. Antennas Propag.*, vol. 67, no. 12, pp. 7633–7636, Dec. 2019.

[26] H. Hashemi, X. Guan, A. Komijani, and A. Hajimiri, "A 24-GHz SiGe phased-array receiver-LO phase-shifting approach," *IEEE Trans. Microw. Theory Techn.*, vol. 53, no. 2, pp. 614–626, Feb. 2005.

[27] S.-S. Jeon, Y. Wang, Y. Qian, and T. Itoh, "A novel smart antenna system implementation for broad-band wireless communications," *IEEE Trans. Antennas Propag.*, vol. 50, no. 5, pp. 600–606, May 2002.

[28] M. Fakharzadeh, S. H. Jamali, P. Mousavi, and S. Safavi-Naeini, "Fast beamforming for mobile satellite receiver phased arrays: Theory and experiment," *IEEE Trans. Antennas Propag.*, vol. 57, no. 6, pp. 1645–1654, Jun. 2009.

[29] G. Han, B. Du, W. Wu, and B. Yang, "A novel hybrid phased array antenna for satellite communication on-the-move in Ku-band," *IEEE Trans. Antennas Propag.*, vol. 63, no. 4, pp. 1375–1383, Apr. 2015.

[30] A. H. Aljuhani, T. Kanar, S. Zihir, and G. M. Rebeiz, "A 256-element Ku-band polarization agile SATCOM receive phased array with wide-angle scanning and high polarization purity," *IEEE Trans. Microw. Theory Techn.*, vol. 69, no. 5, pp. 2609–2628, May 2021.

[31] Z. Duan, Y. Wang, W. Lv, Y. Dai, and F. Lin, "A 6-bit CMOS active phase shifter for Ku-band phased arrays," *IEEE Microw. Wireless Compon. Lett.*, vol. 28, no. 7, pp. 615–617, Jul. 2018.

[32] P. Saha, S. Muralidharan, J. Cao, O. Gurbuz, and C. Hay, "X/Ku-band four-channel transmit/receive SiGe phased-array IC," in *Proc. IEEE Radio Freq. Integr. Circuits Symp. (RFIC)*, Jun. 2019, pp. 51–54.

[33] S. Ghosh and D. Sen, "An inclusive survey on array antenna design for millimeter-wave communications," *IEEE Access*, vol. 7, pp. 83137–83161, 2019.

[34] R. Miura, T. Tanaka, I. Chiba, A. Horie, and Y. Karasawa, "Beamforming experiment with a DBF multibeam antenna in a mobile satellite environment," *IEEE Trans. Antennas Propag.*, vol. 45, no. 4, pp. 707–714, Apr. 1997.

[35] D. Kim, Y. Chi, J. Park, L. Minz, and S. Park, "High-resolution digital beamforming receiver using DDS–PLL signal generator for 5G mobile communication," *IEEE Trans. Antennas Propag.*, vol. 70, no. 2, pp. 1428–1439, Feb. 2022.

[36] Y. Hu et al., "A digital multibeam array with wide scanning angle and enhanced beam gain for millimeter-wave massive MIMO applications," *IEEE Trans. Antennas Propag.*, vol. 66, no. 11, pp. 5827–5837, Nov. 2018.

[37] B. Yang, Z. Yu, J. Lan, R. Zhang, J. Zhou, and W. Hong, "Digital beamforming-based massive MIMO transceiver for 5G millimeter-wave communications," *IEEE Trans. Microw. Theory Techn.*, vol. 66, no. 7, pp. 3403–3418, Jul. 2018.

[38] Y. Yu, W. Hong, Z. H. Jiang, and H. Zhang, "A hybrid radar system with a phased transmitting array and a digital beamforming receiving array," *IEEE Trans. Antennas Propag.*, vol. 69, no. 4, pp. 1970–1981, Apr. 2021.

[39] A. Fukuda, H. Okazaki, and S. Narahashi, "A broadband phased-array antenna system employing frequency-upconverted local signals with phase difference," *IEEE Trans. Microw. Theory Techn.*, vol. 67, no. 1, pp. 383–391, Jan. 2019.

[40] G. D'Amato, G. Avitabile, G. Coviello, and C. Talarico, "DDS-PLL phase shifter architectures for phased arrays: Theory and techniques," *IEEE Access*, vol. 7, pp. 19461–19470, 2019.

[41] P. Chen, W. Hong, H. Zhang, J. Chen, H. Tang, and Z. Chen, "Virtual phase shifter array and its application on Ku band mobile satellite reception," *IEEE Trans. Antennas Propag.*, vol. 63, no. 4, pp. 1408–1416, Apr. 2015.

[42] L. Jiaguo, W. Manqin, J. Xueming, and F. Zhengxing, "Active phased array antenna based on DDS," in *Proc. IEEE Int. Symp. Phased Array Syst. Tech.*, Oct. 2003, pp. 511–516.

[43] Y. Zhang, L. Gao, L. Qi, and W. Wu, "DDS-PLL phased source for Ka-band beam control phased array receiver," in *Proc. 12th Int. Symp. Antennas, Propag. EM Theory (ISAPE)*, Dec. 2018, pp. 1–4.

[44] L. Li, W. Hong, and P. Chen, "Design and implementation of an active antenna array for TD-LTE system based on DDS phase shifter," in *Proc. Asia–Pacific Microw. Conf. Proc. (APMC)*, Nov. 2013, pp. 672–674.

[45] J.-Y. Lee, M.-J. Park, B.-H. Min, S. Kim, M.-Y. Park, and H.-K. Yu, "A 4-GHz all digital PLL with low-power TDC and phase-error compensation," *IEEE Trans. Circuits Syst. I, Reg. Papers*, vol. 59, no. 8, pp. 1706–1719, Aug. 2012.

[46] T. S. Bird, "Definition and misuse of return loss [report of the transactions editor-in-chief]," *IEEE Antennas Propag. Mag.*, vol. 51, no. 2, pp. 166–167, Apr. 2009.

[47] E. W. Herold, R. R. Bush, and W. R. Ferris, "Conversion loss of diode mixers having image-frequency impedance," *Proc. IRE*, vol. 33, no. 9, pp. 603–609, Sep. 1945.

[48] G. Messenger and C. McCoy, "Theory and operation of crystal diodes as mixers," *Proc. IRE*, vol. 45, no. 9, pp. 1269–1283, 1957.

[49] G. Messenger, "New concepts in microwave mixer diodes," *Proc. IRE*, vol. 46, no. 6, pp. 1116–1121, Jun. 1958.
[50] D. M. Pozar, *Microwave Engineering*. Hoboken, NJ, USA: Wiley, 2011.
[51] H. T. Friis, "Noise figure of radio receivers," *Proc. IRE*, vol. 32, no. 7, pp. 419–422, Jul. 1944.
[52] K. Ohmaru and Y. Mikuni, "Direct G/T measurement for satellite broadcasting receivers," *IEEE Trans. Broadcast.*, vol. BC-30, no. 2, pp. 38–43, Jun. 1984.
[53] W. M. Abdel-Wahab et al., "A modular architecture for wide scan angle phased array antenna for K/Ka mobile SATCOM," in *IEEE MTT-S Int. Microw. Symp. Dig.*, Jun. 2019, pp. 1076–1079.
[54] R. C. Monzello, "Unifying G/T and noise figure metrics for receiver systems," in *Proc. Antenna Meas. Techn. Assoc. Symp. (AMTA)*, Nov. 2020, pp. 1–4.
[55] V. Venkateswaran, F. Pivit, and L. Guan, "Hybrid RF and digital beamformer for cellular networks: Algorithms, microwave architectures, and measurements," *IEEE Trans. Microw. Theory Techn.*, vol. 64, no. 7, pp. 2226–2243, Jul. 2016.
[56] I. Ahmed et al., "A survey on hybrid beamforming techniques in 5G: Architecture and system model perspectives," *IEEE Commun. Surveys Tuts.*, vol. 20, no. 4, pp. 3060–3097, 4th Quart., 2018.
[57] Y. Hu, J. Zhan, Z. H. Jiang, C. Yu, and W. Hong, "An orthogonal hybrid analog-digital multibeam antenna array for millimeter-wave massive MIMO systems," *IEEE Trans. Antennas Propag.*, vol. 69, no. 3, pp. 1393–1403, Mar. 2021.
[58] L. Li, W. Hong, Y. Zhang, Z. Chen, and P. Chen, "Design and implementation of an active array antenna with remote controllable radiation patterns for mobile communications," *IEEE Trans. Antennas Propag.*, vol. 62, no. 2, pp. 913–921, Feb. 2014.

**Ye-Eun Chi** received the B.S. degree in electronic engineering from Ewha Womans University, Seoul, South Korea, in 2016, and the M.S. degree from the School of Electrical Engineering, Korea Advanced Institute of Science and Technology (KAIST), Daejeon, South Korea, in 2019, where she is currently pursuing the Ph.D. degree.

Her current research interests include the design of multibeam, beamforming, millimeter-wave antenna system, calibration system, and phased-array antenna system.

**Jinki Park** received the B.S. degree in electronic and electrical engineering with a double major in physics from Sungkyunkwan University, Seoul, South Korea, in 2018, and the M.S. degree in electrical engineering from the Korea Advanced Institute of Science and Technology (KAIST), Daejeon, South Korea, in 2020, where he is currently pursuing the Ph.D. degree.

His current research interests include liquid crystal (LC)-based phased array, holographic antenna, and beamforming techniques at millimeter-wave band.

**Seong-Ook Park** (Senior Member, IEEE) received the B.S. degree from Kyungpook National University, Daegu, South Korea, in 1987, the M.S. degree from the Korea Advanced Institute of Science and Technology (KAIST), Daejeon, South Korea, in 1989, and the Ph.D. degree from Arizona State University, Tempe, AZ, USA, in 1997, all in electrical engineering.

From March 1989 to August 1993, he was a Research Engineer with Korea Telecom, Daejeon, working with microwave systems and networks. He was with the Telecommunication Research Center, Arizona State University, until September 1997. Since October 1997, he has been a Professor with KAIST. His research interests include antenna, radar system, and analytical and numerical techniques in the area of electromagnetics.